

# Multistage Directional Filter Based on Band-Reject Filter With Isolation Improvement Using Composite Right-/Left-Handed Transmission Lines

Jim S. Sun, *Student Member, IEEE*, Humberto Lobato-Morales, *Student Member, IEEE*, Jun H. Choi, *Student Member, IEEE*, Alonso Corona-Chavez, *Senior Member, IEEE*, and Tatsuo Itoh, *Life Fellow, IEEE*

**Abstract**—The  $\lambda/2$  strip-resonator directional filter has good balance between compactness and robustness against manufacturing error. However, there have been difficulties in generalizing the strip-resonator directional filter to realize multipole filtering responses. This paper presents the theory, experiments, and improvement of a new structure of strip-resonator directional filter based on a band-reject filter. This new structure allows the realization of multipole responses and theoretically does not limit the types of filter responses. A three-pole elliptic directional filter prototype is studied thoroughly to show that its performance can be predicted accurately by a conventional filter structure. We also propose a modification of the delay-line part using composite right-/left-handed transmission line to improve the isolation. An isolation level of 30 dB is shown to be achieved consistently.

**Index Terms**—Directional filter (DF), elliptic response, multipole DF.

## I. INTRODUCTION

AS THE frequency spectrum becomes more crowded with various wireless services, high performance channel multiplexing becomes a necessity. Directional filters (DF) are promising candidates for this application and have been the focus of many research efforts [1]–[13]. Compared with other types of multiplexing structures, a DF has the unique trait of wideband matching. This permits the development of the multiplexer system to be done in a module-by-module fashion. This is particularly useful if the number of channels needed is large, where the complexity of using other types of multiplexing structures may become unmanageable [1].

There are three main kinds of DF: hybrid-coupled, traveling-wave loop type, and  $\lambda/2$  strip-resonator type. With hybrid-coupled DFs, the channel filtering response can be completely determined by a bandpass filter design [1], [3]–[5]. This is a desired trait since there is a great deal of research and experience accumulated in conventional filter synthesis [14]–[16], [18]. Also, the circuit construction is relatively easy, since it only requires  $90^\circ$  hybrids and bandpass filters, which

are widely used and studied. However, the drawbacks are its bulkiness and bandwidth limitation. The structure requires a pair of  $90^\circ$  hybrids and a pair of bandpass filters. The increased size and weight may be a problem in a payload-limited platform. Also, the operational bandwidth of the whole multiplexing system is limited by the bandwidth of the  $90^\circ$  hybrids. In [5], an operational fractional bandwidth (FBW) is recorded to be about 50% with a three stage branch-line coupler. Wider bandwidth is achievable, but with the price of additional weight and size of increased stages.

Traveling-wave loop type DFs have also been studied extensively [6]–[9]. Its structure is a lot more compact than the hybrid-coupled type. Also, multistage filtering response has been demonstrated using this structure [6]–[9]. However, unlike the hybrid-coupled directional filter, the traveling-wave loop resonator in this structure is not easy to construct. It is very sensitive to any defect in the manufacturing process. Thus, elaborate tuning effort is usually required [14].

The  $\lambda/2$  strip-resonator-type DF strikes a balance between the compactness and the robustness to manufacturing defects. It does not require  $90^\circ$  hybrid circuits, so it can be more compact than the hybrid-coupled DF. Also, its operational bandwidth can be considerably wider than the hybrid circuits. As will be demonstrated in this paper, an impedance bandwidth of more than 130% can be readily achieved. Compared with a traveling-wave-loop-type structure, it is not as compact but it does not suffer from the ultrahigh sensitivity to manufacturing defects. However, until recent years, realizing a multipole DF response with this structure has not been demonstrated [14].

Realizing a multistage DF response with this structure is the recent research focus. In [10]–[12], the idea of cascading two identical one-pole DFs for a two-stage Butterworth response is experimented and theoretically analyzed. Upon the foundation of these studies, an alternative structure has been proposed in [13]. In this new band-reject filter (BRF)-based structure, two identical BRFs are cascaded to form a DF. A three-pole elliptic DF prototype is presented in [13], demonstrating the extension of the DF response to more than two-stage and response other than Butterworth or Chebyshev. However, the work in [13] is an experimental work. No theory is provided, nor is detailed analysis of the DF performance presented. Also, the deviation of the BRF response realized in the work from the ideal elliptic response is noticeable.

This paper is an extension to the work in [13]. A complete theoretical analysis of this BRF-based structure is presented, and different aspects of the DF performance are examined. We

Manuscript received June 30, 2012; revised September 26, 2012; accepted September 28, 2012. Date of publication November 15, 2012; date of current version December 13, 2012. This paper is an expanded paper from the IEEE MTT-S International Microwave Symposium, Montreal, QC, Canada, June 17–22, 2012.

The authors are with the Department of Electrical Engineering, University of California, Los Angeles, CA 90024 USA (e-mail: b91901018@gmail.com).

Color versions of one or more of the figures in this paper are available online at <http://ieeexplore.ieee.org/author>,

Digital Object Identifier 10.1109/TMTT.2012.2223711

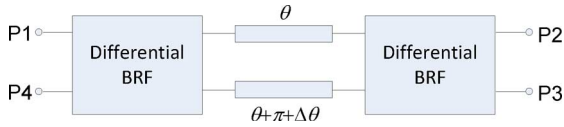


Fig. 1. Basic structure of the BRF-based directional filter.

confirm that there exists a theoretical bound for the rejection level in the filtering response of the DF, and it completely depends on the design of the BRF. Also, there are extra transmission zeros additional to the ones in the BRF response, of which the location can be predicted using the theory presented in this paper. The aforementioned characteristics are validated experimentally by a three-pole elliptic prototype using a new BRF modified from the one in [13]. This new BRF demonstrates a good elliptic response. Excellent correspondence among DF performance, BRF performance, and the theory is confirmed.

In addition to the theoretical study, an improved version of this DF structure is proposed. One potential problem of this BRF-based structure is its isolation level at frequencies other than the center frequency. For the prototypes in [13] and in this paper, this isolation level is around 18 dB. We identify the cause of this low level of isolation and rectify the problem utilizing composite right-/left-handed (CRLH) transmission lines (TL). A new DF prototype using this CRLH technique with the same BRF is fabricated to show the effectiveness of this novel idea.

Another two-pole Chebyshev DF prototype is also presented to demonstrate the capability of this BRF-based structure to realize different filter responses and different numbers of stages. This prototype also demonstrates that the BRF-based structure with the CRLH technique is able to improve the isolation in a specific frequency range. With the two CRLH prototypes in this paper, a wideband isolation level of 30 dB in the intended frequency range is consistently achieved.

## II. BRF-BASED MULTIPOLE DIRECTIONAL FILTER STRUCTURE

### A. Theory

The basic structure for this BRF-based DF is shown in Fig. 1. The differential BRF block is a filtering structure that behaves as a BRF when the upper and lower ports (P1 and P4 in Fig. 1) are excited differentially and as an all-pass filter when excited evenly. At the center frequency, ideally, the delay between the two differential BRFs will have  $180^\circ$  phase difference, so that they switch the excitation mode from common to differential, and vice versa. Here,  $\Delta\theta$  represents the deviation of the phase difference of the two lines from  $180^\circ$  due to the frequency dependence of their phase responses. The working mechanism of this DF structure is illustrated below.

In Fig. 2, we illustrate the situation when the signal frequency is within the rejection bandwidth of the differential BRF. When ports P1 and P4 are excited evenly, the signal will pass through the first differential BRF block since it behaves like an all-pass filter under common excitation. However, the delay lines between the two blocks have  $180^\circ$  phase difference around the center frequency, so the signal becomes differential when it reaches the second differential BRF, and it is reflected back to P1 and P4. When P1 and P4 are under differential excitation, the signal is reflected back to the two ports by the first differential BRF. Under normal working circumstances where only

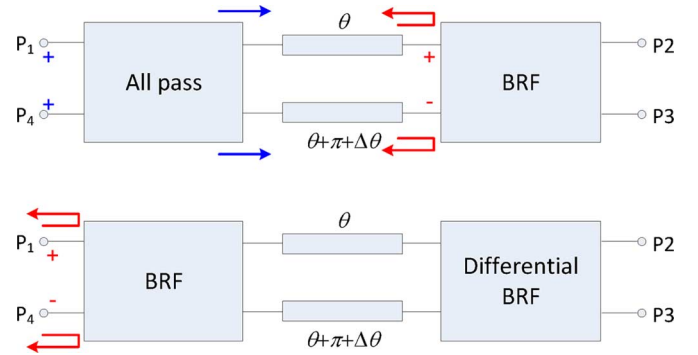


Fig. 2. DF structure under common and differential excitations when the signal frequency is within the rejection bandwidth of the differential BRF.

P1 is excited, the common and differential modes are excited equally, and the two signals reflected back to P1 and P4 will interfere with each other. Thus, we can choose  $\theta$  so that the signals interfere constructively at P4 and destructively at P1. In this way, there would be no input reflection, and the signal in this frequency band is directed to P4.

The previous occurs when the signal frequency is within the BRF rejection bandwidth. If the signal frequency is outside of the BRF bandwidth, it can pass through the differential BRF, hence reaching P2 and P3 regardless of the mode of excitation. If the two modes are excited equally, then they will interfere constructively at P2 and destructively at P3. Thus, when the signal is out of the BRF bandwidth, it goes directly from P1 to P2 and flows into the next stage.

By using the  $S$ -parameters of the differential BRF block to trace the common and differential signal flows in the structure, we can relate the  $S$ -parameter of the final DF with the  $S$ -parameter of the differential BRF, shown as

$$S_{11} = \frac{1}{2} S_{11o} \left\{ 1 + e^{-j(2\theta + \Delta\theta)} \left[ S_{21e} \cos \frac{\Delta\theta}{2} + j S_{21o} \sin \frac{\Delta\theta}{2} \right]^2 \right\} \quad (1a)$$

$$S_{21} = \frac{1}{4} \left( e^{-j\theta} - e^{-j(\theta + \Delta\theta)} \right) (S_{21o} - S_{21e})^2 + e^{-j\theta} S_{21o} S_{21e} \quad (1b)$$

$$S_{31} = \frac{1}{2} (S_{21e}^2 - S_{21o}^2) e^{-j(\theta + 0.5\Delta\theta)} j \sin \frac{\Delta\theta}{2} \quad (1c)$$

$$S_{41} = -\frac{1}{2} S_{11o} \left\{ 1 - e^{-j(2\theta + \Delta\theta)} \left[ S_{21o}^2 \sin^2 \frac{\Delta\theta}{2} + S_{21e}^2 \cos^2 \frac{\Delta\theta}{2} \right] \right\}. \quad (1d)$$

In (1),  $S_{ij}$  is the  $S$ -parameter of the final DF, where  $i, j = 1-4$ . The  $S_{ije}$  and  $S_{ijo}$  are the  $S$ -parameters of the differential BRF under common and differential excitation, respectively. For simplicity, we assume that  $S_{11e} = 0$ , since the structure is of an all-pass nature under common-mode excitation. We can see that  $\Delta\theta$  also affects the DF performance, since when it is not zero the mode switch is not perfect. During this derivation, the multiple reflections between the two differential BRFs are neglected since they have little contribution compared with other terms.

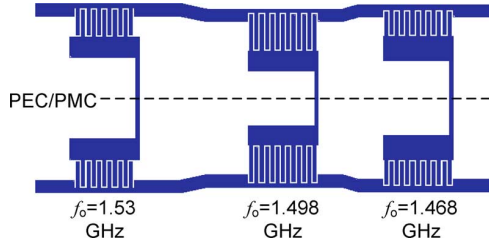


Fig. 3. Elliptic differential BRF on which that the DF is going to be based.

From (1), we can see that the DF function can be achieved by proper selection of the delay  $\theta$ . Around the center frequency, we would want to design  $\Delta\theta$  to be zero so that the mode switch is 100%. Under this condition, the  $\sin \Delta\theta$  terms will be zero and the  $\cos \Delta\theta$  terms will be one. Thus, if we select  $2(\arg S_{21e} + \theta)$  to be an odd multiple of  $\pi$ ,  $S_{11}$  would be zero and  $S_{41}$  would be equal to the  $S_{11o}$  of the differential BRF, where  $\arg S_{21e}$  represents the angle of  $S_{21e}$ . This accomplishes the DF functionality and assures that the filtering response of the final DF will resemble the  $S_{11o}$  response of the differential BRF.

From (1d), we can also see that there are two sources for the transmission zeros in  $S_{41}$  response. The first is the “BRF transmission zero,” which comes from the  $S_{11o}$  response of the BRF. The second one is the “extra transmission zero,” which is caused by the frequency dependency of the transmission line phase, and these extra transmission zeros are in addition to BRF transmission zeros. To see why there are extra transmission zeros, consider when the frequency is not far from the center frequency and  $\Delta\theta$  is small.  $S_{41}$  will be zero at frequencies where  $2(\arg S_{21e} + \theta + \Delta\theta)$  is an even multiple of  $\pi$ . This can also give a quick estimation of the extra transmission zero frequencies around the center frequency.

The major advantage of this DF structure is that the  $S_{41}$  response is bounded by  $S_{11o}$ . This can be observed from (1d), where the  $S_{41}$  response of the DF is  $S_{11o}$  of the differential BRF multiplied by terms of which amplitude is bounded by one. This implies that, when designing the DF to meet certain specifications, considering the design of the differential BRF to meet the specification would be a good start. This reduces the DF synthesis to conventional filter synthesis, where a lot of research and experiences have been accumulated. Also, as mentioned before, extra transmission zeros are introduced at predictable positions. This property can be included into the consideration of choosing the filter response type and number of stages for the differential BRF, which normally results in fewer for the same rejection requirement.

### B. Elliptic Three-Pole Differential BRF

To validate the aforementioned theory, we develop a BRF-based DF prototype with three-pole elliptic response. As mentioned in the previous section, the key to the elliptic DF is to design a differential BRF with the same elliptic response. This differential BRF design with center frequency of 1.5 GHz is shown in Fig. 3. This differential BRF is modified and improved from the similar circuit presented in [13].

When the structure in Fig. 3 is under differential excitation, the symmetrical plane becomes a perfect electric conductor (PEC) plane. The resonators would present a short circuit at

their resonant frequencies, and the circuit behaves as a BRF. The prototype of this BRF, including the resonance frequency of the resonators, strength of coupling to the main TL, and the phase of each TL segments, are derived analytically by following [17]. To realize the elliptical function, the phases of the two line segments are unequal and are  $103^\circ$  and  $79^\circ$ , respectively. However, these phases are supposed to be frequency-independent in theory. To compensate for the frequency variation of the phase in reality, a Gradient optimization is run in ADS to fine tune the BRF prototype. The final result is the resonance frequencies shown in Fig. 3, and the transmission-line (TL) phases of  $99^\circ$  and  $80^\circ$ , respectively.

The final electromagnetic (EM) structure shown in Fig. 3 is arrived by tuning (under differential excitation) the length of the resonators and interdigital capacitors to match the resonance frequencies and coupling strength after the Gradient optimization.

When the structure is under common-mode excitation, the symmetrical plane becomes a perfect magnetic conductor (PMC) plane. The circuit then behaves as a low-pass filter due to the loading presented to the main TL by the interdigital capacitances and the open-ended stubs. Although it is not an all-pass filter as discussed in Section II-A, the cutoff frequency of this low-pass filter is much higher than 1.5 GHz, as will be shown later.

This differential BRF is simulated by Sonnet EM, and the differential and common-mode responses are shown in Fig. 4(a) and (b), respectively. The circuit is simulated with Rogers RO3003 substrate with  $\epsilon_r = 3$  and thickness of 30 mil. The simulation included material and radiation losses.

We can see that, under differential excitation, it is a BRF centered at 1.5 GHz with 5.5% fractional bandwidth (FBW). Furthermore, there are reflection zeros in  $S_{11o}$  response situated at around 1.4 and 1.6 GHz, exhibiting the elliptic response with a side-lobe level of approximately  $-22$  dB. According to the theory presented in (1.d), the  $S_{41}$  of the final DF should also present these BRF transmission zeros at 1.4 and 1.6 GHz and side-lobe level lower than  $-22$  dB.

The theoretical elliptic response is also overlaid for comparison. The correlation between the theoretical and EM simulated response is obvious around the center frequency. The rejection level deviates from the theoretical response below 1 GHz and above 2 GHz because we use real transmission lines to approximate the frequency-independent phase shifts that are needed in theoretical filter prototype [17]. Notice the reflection zero at 2.5 GHz in the simulated response. It is caused by the anti-resonances of the resonators, that is, each branch behaves like an open circuit at this frequency, hence the loading to the main transmission line is minimal.

From Fig. 4(b), we can observe that, when under common-mode excitation, the cutoff frequency of the low-pass structure is higher than 3 GHz. Thus, it should not interfere with the operation of the DF.

### C. Three-Pole Elliptic DF

As mentioned in Section II-A, to construct the DF, we need to select  $\theta$  such that  $2(\arg S_{21e} + \theta)$  is an odd multiple of  $\pi$ . From the simulation for this differential BRF, we found that  $\arg S_{21e}$  is about  $244^\circ$  at 1.5 GHz. Thus, the ideal  $\theta$  for DF construction is estimated to be  $26^\circ$ .

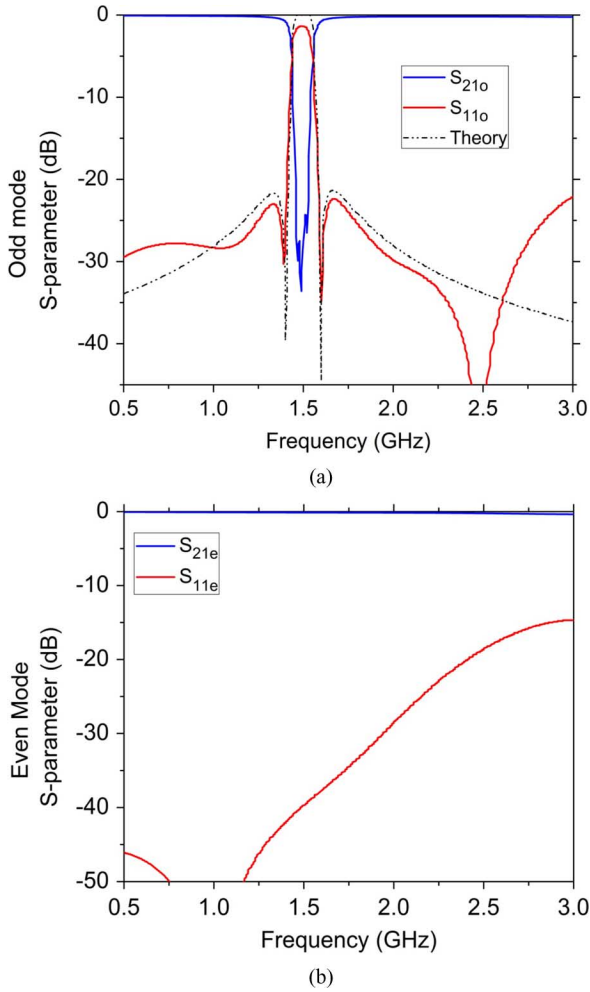


Fig. 4. Response of the differential BRF in Fig. 3 under (a) differential and (b) common-mode excitations.

With this information, we can also estimate the position of the extra transmission zeros in  $S_{41}$  response. As mentioned before, these extra transmission zeros occur at frequencies where  $2(\arg S_{21e} + \theta + \Delta\theta)$  is an even multiple of  $\pi$ . Around 1.5 GHz, we can approximate the frequency variation of  $\arg S_{21e} + \theta$  to be  $(244^\circ + 26^\circ)f/f_o$  using a dispersionless TL model and the frequency variation of  $\Delta\theta$  to be  $(180^\circ)f/f_o$ . Thus, the pair of extra transmission zeros closest to the center frequency can be estimated to be at 1.2 and 1.8 GHz.

This DF uses Rogers RO3003 substrate with  $\epsilon_r = 3$  and thickness of 30 mil, and the fabricated prototype is shown in Fig. 5. The actual length of  $\theta$  is found to be  $27^\circ$  by EM simulation with Sonnet EM, which is very close to the theoretical prediction. Simulated and measured performances of this DF are shown in Fig. 6. The measurements are shown in solid lines, and simulations are shown in dotted lines.

We can see the measurement corresponds to the simulation very well, except for a small frequency shift of about 1.3%. The insertion loss is about 1.2 dB for  $S_{41}$ , and 0.4–0.7 dB for  $S_{21}$ , and the FBW of  $S_{41}$  is about 5%. The BRF transmission zeros in  $S_{41}$  are recorded at 1.42 and 1.62 GHz in Fig. 6(a), which correlate very well with the response of the differential BRF and confirm the earlier theoretical analysis of (1.d). Also, the extra transmission zeros in  $S_{41}$  are also observed. The pair of extra

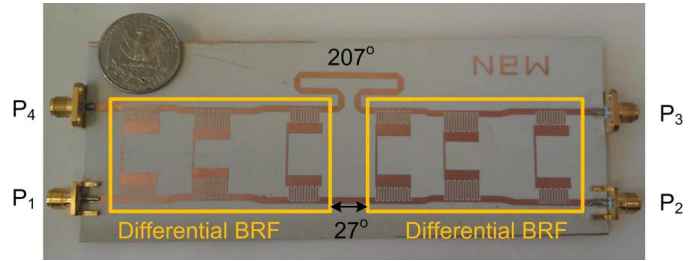


Fig. 5. Photograph of the constructed BRF-based DF using the differential BRF in Fig. 3.

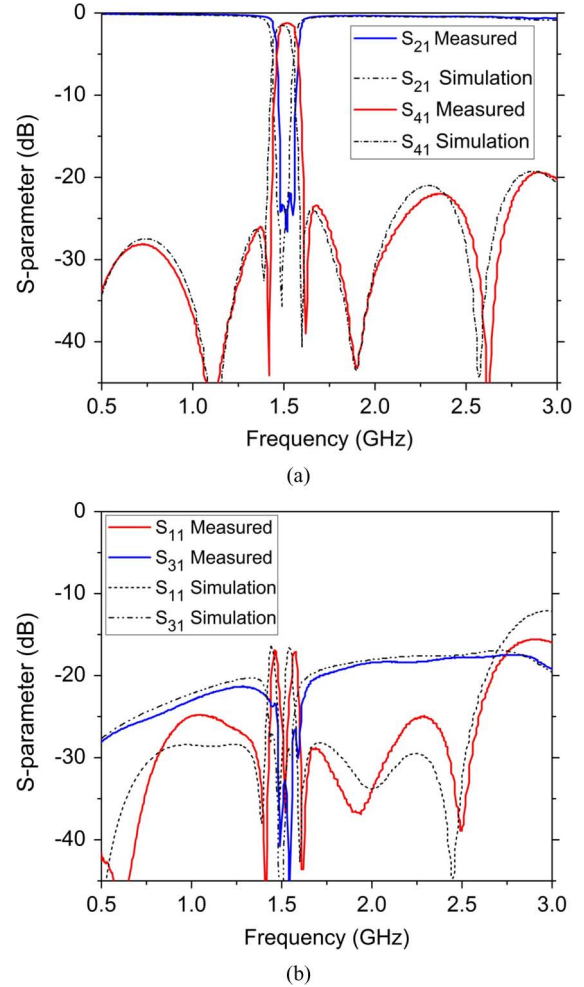


Fig. 6. Measured  $S$ -parameters of the three-pole elliptic directional filter prototype.

transmission zeros that are closest to the center frequency are located at 1.1 and 1.9 GHz, which are close to the earlier prediction with deviation less than 8.5%. The deviation mainly comes from the assumption of  $\Delta\theta = 0$ . The frequencies of this transmission zero pair is about 27% away from the center frequency, and this assumption is not entirely true. However, it still serves as a good estimation of the positions of this transmission zero pair. If accurate prediction for transmission zero frequencies is desired, then the full formula for  $S_{41}$  in (1d) should be used.

Fig. 6(b) shows the  $S_{11}$  and  $S_{31}$  response of the DF. We can see that within a bandwidth of 130%, the structure has  $S_{11}$  lower

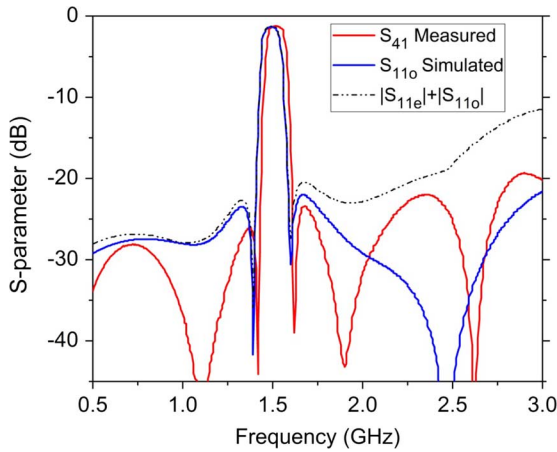


Fig. 7.  $S_{41}$  filtering response of the DF overlaid with  $S_{11o}$  of the differential BRF and the modified bound for  $S_{41}$  in practice.

than  $-17$  dB and isolation between ports P3 and P1 better than 18 dB.

Finally, it is important to examine how well the claim that the  $S_{41}$  will be bounded by  $S_{11o}$  of the differential BRF applies in practice. In Fig. 7, we show the measured  $S_{41}$  response of the DF overlaid with the simulated  $S_{11o}$  of the differential BRF in Fig. 4(a). We can see that, at the lower frequencies side from the center frequency,  $S_{41}$  is truly bounded by  $S_{11o}$  of the BRF. However, at higher frequency ranges, the  $S_{41}$  has ripple levels that exceed  $S_{11o}$  at some frequencies. This is because when deriving (1a)–(1d),  $S_{11e}$  of the differential BRF is assumed to be zero. By observing the  $S_{11e}$  of the realized differential BRF in Fig. 4(b), we can see that, at frequencies higher than 2 GHz, the level of  $S_{11e}$  exceeds the rejection level of  $S_{11o}$  and becomes the dominant factor. By going through similar theoretical derivation but including the effect of  $S_{11e}$ , one can show that, in practice, the absolute bound of  $S_{41}$  should be as shown in

$$|S_{41}| < (|S_{11o}| + |S_{11e}|). \quad (2)$$

This modified bound is also overlaid in Fig. 7.

This observation shows that the rejection level of  $S_{41}$  filtering function is also affected by the  $S_{11e}$  of the differential BRF. Thus, in a system where particularly high rejection is needed, one must also pay close attention to the level of  $S_{11e}$ . However, because of the additional transmission zero pair, the rejection level of  $S_{41}$  will generally be better than  $S_{11o}$  up to the frequency of the first additional transmission zero. In this prototype, it is shown that the  $S_{41}$  filtering response has better rejection level than  $S_{11o}$  does up to  $1.35f_o$ .

### III. ISOLATION IMPROVEMENT BASED ON CRLH

When observing the performance of the DF prototype in Fig. 6, one can notice that the isolation between P1 and P3 is very good around the center frequency but degrades pretty rapidly at other frequencies. Fig. 6 shows isolation levels around 18 dB at higher frequencies. This may not be a problem if all of the channels in the multiplexing system are receiving channels but might be a problem if some channels are transmitting with high power using a common antenna with the receiving channels.

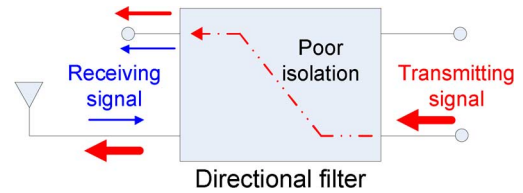


Fig. 8. Potential problem of a DF if the isolation level is not high.

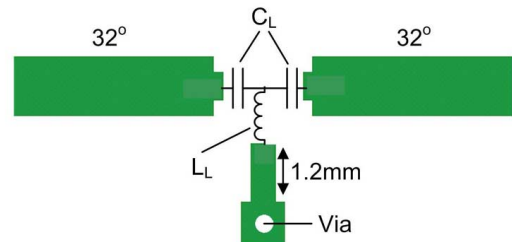
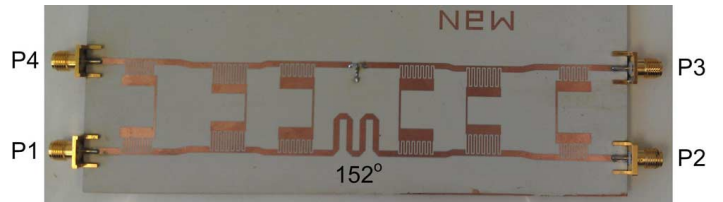


Fig. 9. Photograph of the DF incorporating CRLH phase matching, and the realization of CRLH transmission line.

This situation is shown in Fig. 8, showing that the receiving signal would be interfered by a poorly isolated strong transmitting signal. Thus, here, we present a way to increase the isolation level to alleviate this problem while keeping other desirable advantages.

By observing the formulation of  $S_{31}$  in (1c), we found that the isolation level is directly proportional to  $\sin \Delta\theta/2$ . Although we design the  $\Delta\theta$  to be zero at the center frequency, it increases as we move away from the center frequency because of the difference in the phase slope of the two microstrip delay lines. Thus, the isolation performance is very good at the center frequency where  $\Delta\theta$  is zero but becomes poorer away from the center frequency.

CRLH TLs have been studied extensively due to their ability to have their phase engineered [19]–[21]. In [21], the authors demonstrate the concept of matching the phase slope of a CRLH line to a microstrip line. Here, we adopt this concept to match the phase slope of the two different delay lines, so that  $\Delta\theta$  is maintained to be small over a wider frequency range. However, here we face a restriction that  $\theta$  is a predetermined delay for directionality performance, where in [21] it is a design freedom.

The DF prototype incorporating the CRLH phase-matching scheme is shown in Fig. 9. It uses the same differential BRF shown in Fig. 3. Note that, because  $\theta = 27^\circ$  in the original design is too short to work with the CRLH line, the differential BRF at the right is flipped. Since the simulated  $S_{11o}$  and  $S_{22o}$  of the differential BRF has the same amplitude but  $247^\circ$  phase difference at center frequency, theoretically,  $\theta$  should be chosen as  $150^\circ$  at 1.5 GHz instead of  $27^\circ$ . In EM simulation, we found this delay to be  $152^\circ$ , as shown in Fig. 9, which is very close to the theoretical value.

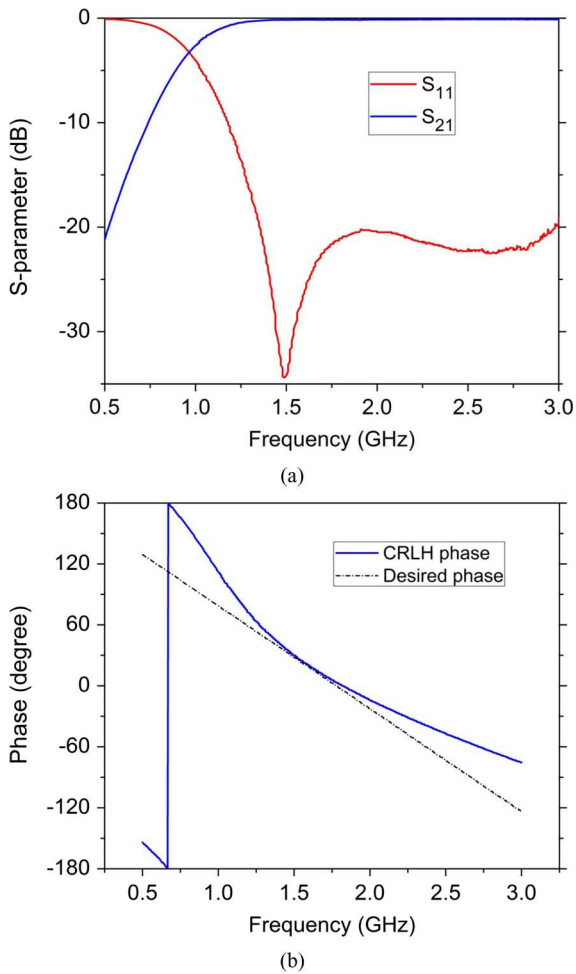


Fig. 10. (a)  $S$ -parameter and (b) the phase response of the CRLH transmission.

This  $152^\circ$  delay is realized by the microstrip line. Thus the other delay line will be designed as a CRLH transmission line with  $28^\circ$  phase advance at 1.5 GHz and the same phase slope as a  $152^\circ$  microstrip line.

The realization of the CRLH line part of this DF is also shown in Fig. 9. A single unit cell of the left-hand transmission line is in the middle of the structure. The series capacitor  $C_L$  is realized by a surface mount capacitor of 2.2 pF, and the shunt inductance is realized by a surface mount inductor  $L_L$  of 4.7 nH plus a short section of shorted stub. The right-hand part is realized by 50- $\Omega$  microstrip lines with  $32^\circ$  delay. The structure is designed so that we obtain the best matching at the center frequency of 1.5 GHz with the desired phase delay and phase slope.

The simulated performance of this CRLH line is shown in Fig. 10, where the amplitude of its  $S$ -parameter is shown in Fig. 10(a), and the phase response of its  $S_{21}$  is shown in Fig. 10(b). The desired phase response to match that of the microstrip line is also shown in Fig. 10(b) for comparison. We can see that the structure is of high-pass nature with cutoff frequency around 1.25 GHz, and has a zero in  $S_{11}$  around 1.5 GHz. The phase of the structure is  $30^\circ$  at 1.5 GHz, and follows the desired phase response closely.

The improvement of using this CRLH phase-matching scheme over the conventional case can be clearly seen in Fig. 11, where the magnitude of  $\Delta\theta$  is plotted for both the

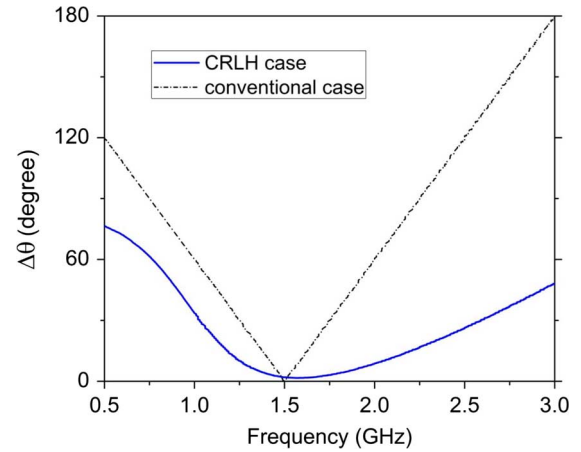


Fig. 11.  $\Delta\theta$  comparison between the directional filter with and without the CRLH phase matching.

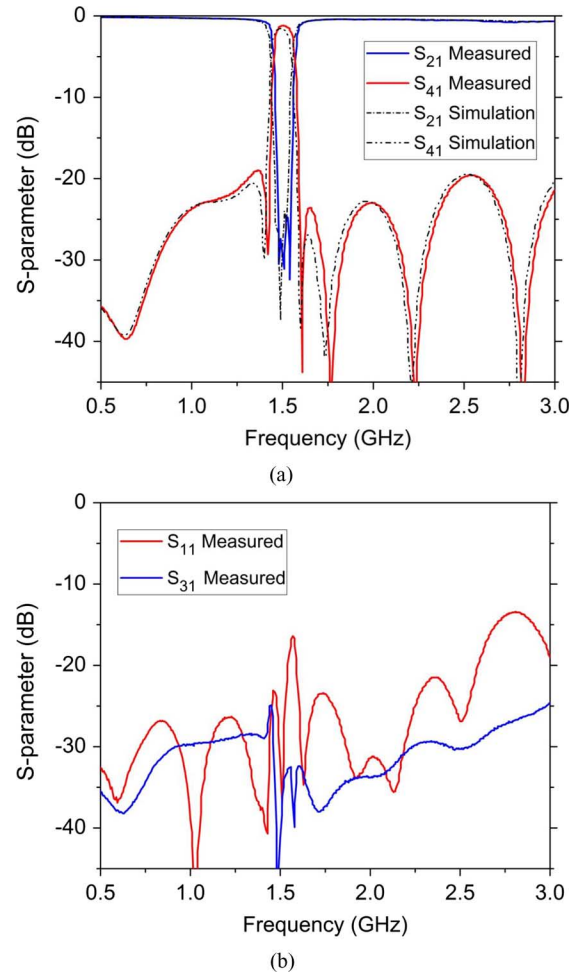


Fig. 12.  $S$ -parameter response of the DF with CRLH phase matching, exhibiting high isolation.

conventional case and the CRLH case. For a wide frequency range of 0.5–3 GHz, the CRLH case demonstrates less  $\Delta\theta$  than the conventional case does.

The simulated and measured performance of this DF prototype using CRLH phase matching is shown in Fig. 12. The measured and simulated  $S_{21}$  and  $S_{41}$  response is shown in

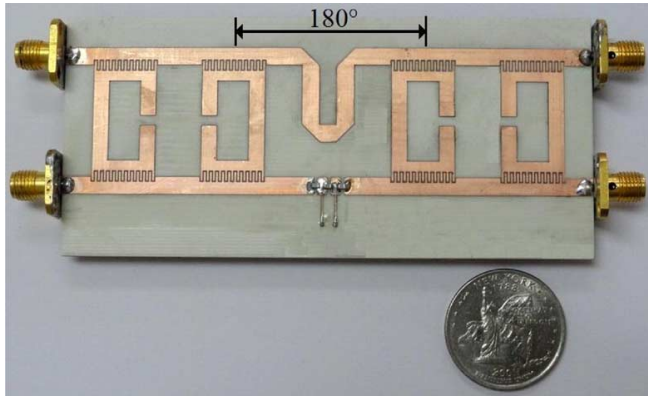


Fig. 13. Photograph of the two-stage DF with CRLH phase matching.

Fig. 12(a). The measurement corresponds very well with the simulation, and the sharp elliptic filtering response is preserved. Also, the extra transmission zeros appear more frequently and are closer to the center frequency. This is due to the larger  $\theta$  that we used in this design. Since larger  $\theta$  at 1.5 GHz results in larger phase slope, the period of which the additional zeros appear is reduced. The matching and isolation of this DF is shown in Fig. 12(b). Only the measured responses are shown for the clarity of the figure. The structure is well matched with  $S_{11}$  lower than  $-12$  dB, and the isolation maintains a level around  $-30$  dB for a very wide frequency range. Compared with the isolation performance of the conventional case in Fig. 6, it shows an improvement over 12 dB.

In high-power applications, the insertion loss is critical. However, compared with the three-stage prototype without CRLH phase matching, the insertion loss only increased by a maximum of  $\sim 0.25$  dB across the frequency band of 0.5–3 GHz.

Finally, we present a design of a two-stage DF with CRLH phase matching to demonstrate the difference in the DF design with different BRF structures and different numbers of poles and the ability of emphasizing isolation at different frequency ranges using this CRLH phase matching scheme.

Fig. 13 shows the realized two-stage DF prototype. It is based on a two-stage Chebyshev BRF with a center frequency of 1.5 GHz. Notice that, because of the fewer stages in the BRF, the phase delay in  $S_{11e}$  is actually a lot shorter (ideally  $90^\circ$ ). Thus, to achieve the proper directionality, a longer delay line of  $\theta = 180^\circ$  is needed. This length works well with the CRLH phase-matching scheme, unlike the three-stage prototype where the flip of the second differential BRF is required.

The design of the CRLH part of this DF emphasizes isolation in the frequency range higher than the center frequency. It uses two unit cells of the left-handed section in between the microstrip lines, with series capacitors realized by surface-mount components of 3.9 pF on the two sides and 2 pF in the middle. The 5.1-nH shunt inductance needed in the CRLH structure is realized by shorted stubs. The  $\Delta\theta$  plot for this CRLH line is shown in Fig. 14. We can see that  $\Delta\theta$  is designed so that it is smaller than  $15^\circ$  in the frequency range higher than 1.5 GHz. Thus, we expect the isolation will be better in this spectrum range.

This DF is fabricated on a Rogers RO4003 substrate with  $\epsilon_r = 3.55$  and thickness of 60 mil. Split-ring resonators are used

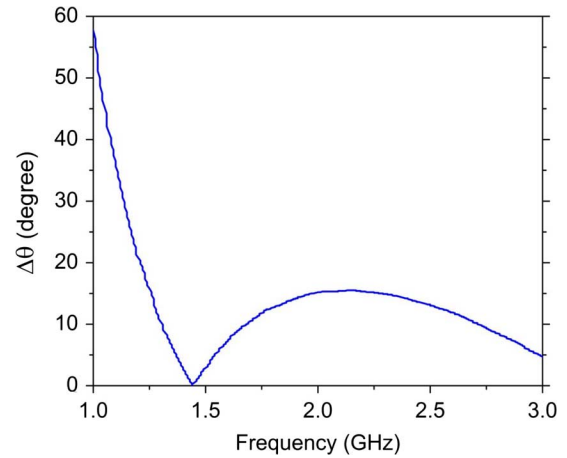
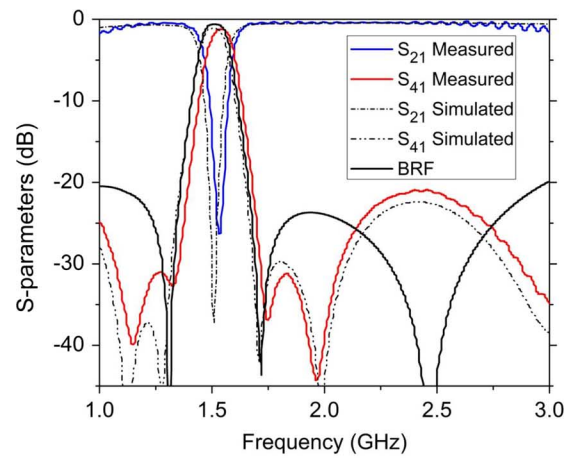
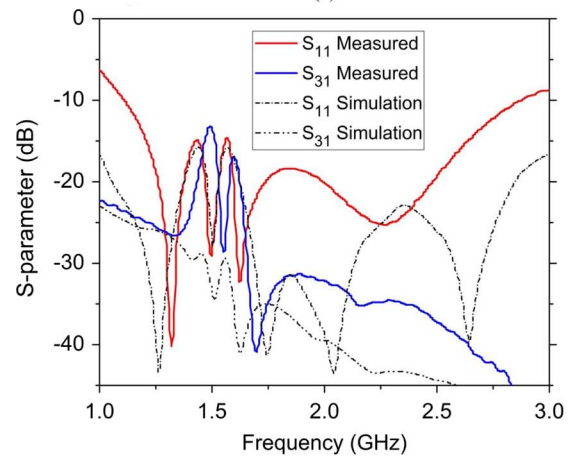


Fig. 14. Magnitude of  $\Delta\theta$  of the CRLH design in the two-stage DF prototype.



(a)



(b)

Fig. 15. Simulated and measured  $S$ -parameter of the two-stage DF prototype.

and capacitively coupled to the two transmission lines by interdigital fingers. This DF is designed to have a center frequency of 1.5 GHz with 8% FBW.

The simulated and measured  $S$ -parameter responses of this DF are shown in Fig. 15. The  $S_{21}$  and  $S_{41}$  responses are shown in Fig. 15(a) overlaid with the simulated response of the differential BRF in the solid black curve. The measurement corresponds to the simulation very well. It can be clearly observed

that the transmission zeros in  $S_{41}$  around 1.3 and 1.75 GHz are the BRFB transmission zeros, and those at 1.15 and 1.96 GHz are the extra transmission zero introduced by the BRFB-based DF structure. It is noted that the locations of these extra zeros are very close to the extra zeros of the conventional three-stage DF prototype in Fig. 6(a), which are 1.1 and 1.9 GHz. This is because  $\arg S_{11e} + \theta$  is  $270^\circ$  in both cases, and the location of the first additional zero pair is dominated by this factor.

In Fig. 15(b), we show the measured and simulated  $S_{11}$  and  $S_{31}$  responses. The structure demonstrates wideband matching from 1.2 to 2.7 GHz. Notice that the isolation is better in the frequency range higher than in the center frequency, as was intended by the design of the CRLH line. It measured at least 30 dB in this frequency range and increases with frequency.

#### IV. CONCLUSION

In this paper, we give a detailed analysis of the multistage DF structure proposed in [13]. The  $S_{41}$  filtering response resembles the  $S_{11o}$  response of the differential BRFB on which it is based. Moreover, the structure is capable of generating extra transmission zeros in the  $S_{41}$  response at predictable locations, thus increasing the rejection level in the stopband. The rejection level is theoretically limited by the common-mode matching  $S_{11e}$  of the differential BRFB, but the three-stage prototype still demonstrates a low rejection level within a 70% FBW thanks to good  $S_{11e}$  and extra transmission zeros. From the multiplexer design point of view, this means that, in order for the DF to meet the channel filtering requirement, it is sufficient to design the differential BRFB to meet the specifications. This reduces the DF response design to the BRFB design, which has been extensively researched and experimented.

One potential problem of this multistage DF structure is that the isolation level may not be sufficiently high at frequencies other than the center frequency. The original prototype demonstrates an isolation level around 18 dB. This can be rectified by applying CRLH phase matching for the delay lines connecting the two differential BRFBs with a small penalty in insertion loss ( $\sim 0.25$  dB). For the intended frequency range, a wideband isolation level of 30 dB can be consistently achieved, as verified by the two- and three-stage prototypes.

#### REFERENCES

- [1] D. S. Levinson and R. L. Bennett, "Multiplexing with high performance directional filters," *Microw. J.*, pp. 99–112, June 1989.
- [2] S. B. Cohn and F. S. Coale, "Directional channel-separation filters," in *Proc. IRE*, 1956, vol. 44, no. 8, pp. 1018–1024.
- [3] J.-S. Hong, M. J. Lancaster, R. B. Greed, D. Jedamzik, J.-C. Mage, and H. J. Chaloupka, "A high-temperature superconducting duplexer for cellular base-station applications," *IEEE Trans. Microw. Theory Tech.*, vol. 48, no. 8, pp. 1336–1343, Aug. 2000.
- [4] S. H. Talisa, M. A. Janocko, D. L. Meier, C. Moskowitz, R. L. Grassel, and J. Talvacchio, "High-temperature superconducting four-channel filterbanks," *IEEE Trans. Appl. Supercond.*, vol. 5, no. 2, pt. 3, pp. 2079–2082, Jun. 1995.
- [5] T. K. Kataria, S.-P. Sun, A. Corona-Chavez, and T. Itoh, "New approach to hybrid multiplexer using composite right-left handed lines," *IEEE Microw. Wireless Compon. Lett.*, vol. 21, no. 11, pp. 580–582, Nov. 2011.
- [6] F. S. Coale, "A traveling-wave directional filter," *IRE Trans. Microw. Theory Tech.*, vol. 4, no. 4, pp. 256–260, 1956.
- [7] J. L. B. Walker, "Exact and approximate synthesis of TEM-mode transmission-type directional filters," *IEEE Trans. Microw. Theory Tech.*, vol. MTT-26, no. 3, pp. 186–192, Mar. 1978.

- [8] S. Uysal, "Microstrip loop directional filter," *Electron. Lett.*, vol. 33, no. 6, pp. 475–476, 1997.
- [9] Y. Cheng, W. Hong, and K. Wu, "Half mode substrate integrated waveguide (HMSIW) directional filters," *IEEE Microw. Wireless Compon. Lett.*, vol. 17, no. 7, pp. 504–506, Jul. 2007.
- [10] H. Lobato-Morales, A. Corona-Chavez, J. L. Olvera-Cervantes, and D. V. B. Murthy, "Multi-pole microstrip directional filters for multiplexing applications," in *Proc. Int. Conf. Electr. Commun. Comput.*, 2011, pp. 344–349.
- [11] H. Lobato-Morales, A. Corona-Chavez, T. Itoh, and J. L. Olvera-Cervantes, "Dual-band multi-pole directional filter for microwave multiplexing applications," *IEEE Microw. Wireless Compon. Lett.*, vol. 21, no. 12, pp. 643–645, Dec. 2011.
- [12] J. P. Kim, "Improved design of single-section and cascade planar directional filters," *IEEE Trans. Microw. Theory Tech.*, vol. 59, no. 9, pp. 2206–2213, Sep. 2011.
- [13] J. S. Sun, H. Lobato-Morales, A. Corona-Chavez, and T. Itoh, "New approach to multi-stage directional filter based on band-reject filter design," in *IEEE MTT-S Int. Microw. Symp. Dig.*, Montreal, QC, Canada, Jun. 17–22, 2012, pp. 1–3.
- [14] G. L. Matthaei, L. Young, and E. M. T. Jones, *Microwave Filters, Impedance-Matching Networks, and Coupling Structures*. Norwood, MA: Artech House, 1980.
- [15] R. J. Cameron, "General coupling matrix synthesis methods for Chebyshev filtering function," *IEEE Trans. Microw. Tech.*, vol. 47, no. 4, pp. 433–441, Apr. 1999.
- [16] S. Amari and M. Bekheit, "Physical interpretation and implications of similarity transformations in coupled resonator filter design," *IEEE Trans. Microw. Theory Tech.*, vol. 55, no. 6, pp. 1139–1153, Jun. 2007.
- [17] J. D. Rhodes, "Waveguide bandstop elliptic function filters," *IEEE Trans. Microw. Theory Tech.*, vol. MTT-20, no. 11, pp. 715–718, Nov. 1972.
- [18] J.-S. G. Hong and M. J. Lancaster, *Microwave Filters for RF/Microwave Applications*. New York: Wiley, 2001.
- [19] C. Caloz and T. Itoh, "Novel microwave devices and structures based on the transmission line approach of meta-materials," in *IEEE MTT-S Int. Microw. Symp. Dig.*, 2003, pp. 195–198.
- [20] H. V. Nguyen and C. Caloz, "Metamaterial-based dual-band six-port front-end for direct digital QPSK transceiver," in *Proc. Electrotechnical Conf.*, 2006, pp. 363–366.
- [21] C.-J. Lee, K. M. K. H. Leong, and T. Itoh, "Metamaterial transmission line based bandstop and bandpass filter designs using broadband phase cancellation," in *IEEE MTT-S Int. Microw. Symp. Dig.*, 2006, pp. 935–938.



**Jim S. Sun** (S'08) received the B.S. degree from National Taiwan University, Taipei, Taiwan, in 2006, and the M.S. degree from the University of California, Los Angeles, in 2008, where he is currently working toward the Ph.D. degree.

He has been a Graduate Student Researcher with the Microwave Electronics Laboratory, University of California, Los Angeles, since 2007, and his research activity includes conformal retro-directive array in the M.S. program and tunable filters, directional filters, composite right-/left-handed transmission lines,

and antenna design in doctoral program.



**Humberto Lobato-Morales** (S'05) received the B.Sc. and M.Sc. degrees from Universidad de las Américas-Puebla, Puebla, México, in 2006 and 2008, respectively. He is currently working toward the Ph.D. degree in electronics engineering at Instituto Nacional de Astrofísica, Óptica y Electrónica, Puebla, México.

In 2008, he joined the Emerging Microwave Technologies Group (EMT), Instituto Nacional de Astrofísica, Óptica y Electrónica, Puebla, México, as a Research Engineer. In 2011, he was a Visiting

Student with the University of California, Los Angeles. His research interests include microwave filters and multiplexers, microwave metamaterials, material characterization using microwaves, and remote sensing systems.



**Jun H. Choi** (S'12) received the B.S. degree from the University of California, Irvine, in 2003, the M.S. degree from the University of California, Los Angeles, in 2007, where he is currently working toward Ph.D. degree, all in electrical engineering.

His research interests include phased-array systems, microwave/millimeter-wave circuit designs, and devices based on composite right-/left-handed and metamaterial structures.



**Alonso Corona-Chavez** (SM'09) received the B.Sc. degree in electronics engineering from the Instituto Tecnológico y de Estudios Superiores de Monterrey, Mexico City, Mexico, in 1997, and the Ph.D. degree from the University of Birmingham, Birmingham, U.K., in 2001. His dissertation concerned microwave beamformers using high-temperature superconductors.

From 2001 to 2004, he was a Microwave Engineer for CryoSystems Ltd. (U.K.), where he developed superconducting front-ends for the telecommunications industry. Moreover, he was an Honorary Research Fellow with the Electrical Engineering Department, University of Birmingham, Birmingham, U.K. (2001–2004). In September 2004, he joined the Large Millimeter Telescope, Instituto Nacional de Astrofísica, Óptica y Electrónica, Puebla, México, where he is currently a Professor with the Electronics Department. In April 2009, he was awarded a Fulbright fellowship to carry out research at the Electrical Engineering Department, University of California at Los Angeles.

Dr. Corona is a senior member of the Institution of Engineering and Technology and a member of the National Systems for Researchers.



**Tatsuo Itoh** (S'69–M'69–SM'74–F'82–LF'06) received the Ph.D. degree in electrical engineering from the University of Illinois at Urbana-Champaign, Urbana, in 1969.

After working for the University of Illinois, SRI, and the University of Kentucky, he joined the faculty at The University of Texas at Austin in 1978, where he became a Professor of electrical engineering in 1981. In September 1983, he was selected to hold the Hayden Head Centennial Professorship of Engineering at The University of Texas. In January 1991, he joined the University of California, Los Angeles, as a Professor of electrical engineering and holder of the TRW Endowed Chair in Microwave and Millimeter Wave Electronics (currently Northrop Grumman Endowed Chair). He has authored and coauthored 400 journal publications, 820 refereed conference presentations, and 48 books/book chapters in the area of microwaves, millimeter-waves, antennas and numerical electromagnetics. He has generated 73 Ph.D. students.

Dr. Itoh is a member of the Institute of Electronics and Communication Engineers of Japan and Commissions B and D of USNC/URSI. He served as the editor of the IEEE TRANSACTIONS ON MICROWAVE THEORY AND TECHNIQUES from 1983 to 1985. He was President of the IEEE Microwave Theory and Techniques Society (MTT-S) in 1990. He was the Editor-in-Chief of the IEEE MICROWAVE AND GUIDED WAVE LETTERS from 1991 through 1994. He was elected as an Honorary Life Member of the IEEE MTT-S in 1994. He was the Chairman of Commission D of International URSI from 1993 to 1996. He serves on advisory boards and committees of a number of organizations. He served as a Distinguished Microwave Lecturer on Microwave Applications of Metamaterial Structures of IEEE MTT-S from 2004 to 2006. He received a number of awards including IEEE Third Millennium Medal in 2000, and IEEE MTT Distinguished Educator Award in 2000. He was elected to a member of National Academy of Engineering in 2003. In 2011, he received Microwave Career Award from the IEEE MTT-S.